

Investigation of Computational Flow Field over a Re-entry Capsule at High Speed

S. Rathnavel

Assistant Professor
Department of Aeronautical Engineering
Rajadhani Institute of Engineering
Nagaroor, Kerala,
India

K. Balaji

Project Engineer
KCIRI, Coimbatore
India

Prem Kumar P. S.

Associate professor
Department of Aeronautical Engineering
Kumaraguru college of Engineering
Coimbatore
India

N. Sathesh Raja

Assistant Professor
Department of Aeronautical Engineering
Rajadhani Institute of Engineering
Nagaroor, Kerala
India

K. Vijaya Sankaran

VESRAD Technologies PVT Ltd.
Kalpakkam
India

Manned space programme has become inevitable in the modern world. One important aspect in such endeavors is getting the crew back to home safe and sound. Re-entry capsules are widely used for bringing back astronauts back to the Earth. The re-entry mission is a very crucial one, with speeds up to 30 times than that of sound and temperatures hot enough to ionize air. The study and design of a re-entry capsule has to be done with utmost concern over the life of returning asronauts. In this paper, simulations carried out over a re-entry vehicle for various free-stream conditions such as subsonic, supersonic and hypersonic flow regimes. Results were obtained by solving compressible Navier-Stokes equation with k-omega turbulent model. Simulations were carried out for various inlet conditions corresponding to an altitude of a re-entry vehicle by using CFD code SU2. The geometrical parameters of a re-entry vehicle such as spherical nose radius and cone angle were varied and the effects of the aerodynamic phenomena such as shock wave, flow separation and wake formation over a downstream of a module were studied. In this paper, the results pertaining to the pressure distribution, the Mach contour and temperature over a module is presented.

Keywords: Computational fluid dynamics, Re-entry vehicle, shock wave disturbance, Turbulent flow

1. INTRODUCTION

After the space mission, a re-entry capsule returns to the Earth atmosphere. At that time, the speed of the re-entry capsule is very high and the speed gradually decreases with altitude. The shape of the capsule is generally selected after aerodynamic and thermal consideration. The fore-body of the capsule has a spherical nose which is aerodynamically more stable than other shapes [1]. Due to the shape of the nose, it produces high aerodynamic drag which affects the capsule. The shoulder radius (Frontal area) and flare angle in capsule have a significant influence on the fore body and the position of flow separation point [2]. Allen and Cheng [10] carried out the numerical simulation in re-entry module and studied the flow separation in which is observed experimentally earlier.

From the investigations [6], it is evident that aerodynamic data generation is possible by the following methods like Analytical method, CFD codes and Wind tunnel testing

In our present work, geometrical parameters of a capsule such as radius of the spherical nose and cone angle were varied. The effects over the capsule such as shock stand-off distance and the flow separated wake region behind the capsule were investigated.

2. MATHEMATICAL FORMULATION

The 3-D fluid flow is governed by 3-D Navier Stokes (NS) equations which comprise continuity, momentum and energy equations.

The integral formulations of the three conservation equations are given below. This equation represents the integral form of the continuity equation, which is based on the law of mass conservation [6].

$$\frac{\partial}{\partial t} \int_{\Omega} \rho d\Omega + \int_{\Omega} \rho (\vec{v}, \vec{n}) ds = 0 \quad (1)$$

where, ρ is the density of fluid, \vec{v} is the velocity of the vector, \vec{n} is the unit normal vector, dS is the elemental surface area and Ω is the control volume.

The expression for the momentum conservation inside an arbitrary control volume Ω which is fixed in space and is given by

$$\frac{\partial}{\partial t} \int_{\Omega} \rho \vec{v} d\Omega + \int_{\partial\Omega} \rho \vec{v} (\vec{v}, \vec{n}) ds = \int_{\Omega} \rho \vec{f}_e d\Omega - \int_{\partial\Omega} \rho \vec{n} ds + \int_{\partial\Omega} \rho \vec{\tau}, \vec{n} \quad (2)$$

where \vec{f}_e is the body force term, $\vec{\tau}$ is the viscous stress tensor.

The energy conservation equation is given below.

$$\dot{q}_h \quad (3)$$

where H is the total enthalpy, E is the total energy per unit mass, k is the thermal diffusivity coefficient, T is

Received: August 2019, Accepted: April 2020

Correspondence to: S.Rathnavel, Assistant Professor,
Department of Aeronautical Engineering, Rajadhani
Institute of Engineering and Technology, Kerala, India.

E-mail: rathnavelaero@gmail.com

doi: 10.5937/fme2003551R

© Faculty of Mechanical Engineering, Belgrade. All rights reserved

FME Transactions (2020) 48, 551-556 551

the absolute temperature and \dot{q}_h is the heat transfer per unit mass.

Finite volume formulation is given in integral form to solve the equation with SU2 [6, 8] as follows

$$\frac{\partial}{\partial t} \int U dV + \int (F_c - F_v) ds = Q \quad (4)$$

$$F_c = \begin{bmatrix} \rho H V \\ \rho u V + n_x P \\ \rho v V + n_y P \\ \rho w V + n_z P \\ \rho V \\ \rho k V \\ \rho \varepsilon V \\ \rho z V \end{bmatrix} \quad F_v = \begin{bmatrix} n_x \theta_x + n_y \theta_y + n_z \theta_z \\ n_x \tau_{xx} + n_y \tau_{yy} + n_z \tau_{zz} \\ n_x \tau_{yx} + n_y \tau_{yy} + n_z \tau_{yz} \\ n_x \tau_{zx} + n_y \tau_{zy} + n_z \tau_{zz} \\ 0 \\ \left(\mu_l + \frac{\mu_t}{\sigma_k} \right) \frac{\partial k}{\partial x_j} \\ \left(\mu_l + \frac{\mu_t}{\sigma_\varepsilon} \right) \frac{\partial \varepsilon}{\partial x_j} \\ \left(\frac{\mu_l}{pr} + \frac{\mu_t}{\sigma_k} \right) z \end{bmatrix} \quad (5)$$

The dynamic viscosity is defined as a sum of molecular viscosity (μ_l) and turbulent viscosity. Therefore,

$$\mu = \mu_l + \mu_t \quad (6)$$

Molecular viscosity μ_l by using Sutherland law is given by,

$$\mu_l = \mu_{ref} \left(\frac{T}{T_{ref}} \right)^{1.5} \left(\frac{T + S}{T_{ref} + S} \right) \quad (7)$$

Turbulence Viscosity is given by,

$$\mu_t = \frac{c \mu \rho k^2}{\varepsilon} \quad (8)$$

Static pressure downstream of shock wave is analytically determined by [9]

$$\frac{P_2}{P_1} = 1 + \frac{2\gamma}{\gamma + 1} (M_1^2 - 1) \quad (9)$$

where P_1 refers to pressure at upstream region of the shock and P_2 refers to pressure at downstream region of the shock.

3. GRIDS AND COMPUTATIONAL DOMAIN

The design of the re-entry vehicle was adapted from Mehta [1] and the design was varied to study the effects of the nose radius and cone angle over the entire vehicle. The vehicle is moving at an arbitrary angle of attack; instead of an axisymmetric body, a 2D cut section of the vehicle was considered. Grids were clustered adjacent to the vehicle model to capture the flow field accurately near the wall. Structured grids were used since it requires low computational time and also based on the design. The grid details are given in Table 1.

Table 1: Grid Details

Type	Structured Grid
First cell height	6 microns
Number of cells	37,500
Spacing	Geometric stretching with factor 1.1

To model the flow near the walls with accuracy, the first grid point from the surface should be within the viscous sub-layer. Fig 1 shows a zoomed view over a re-entry module. The first cell height in the normal direction of the body surface is fixed at 6 micron. The domain size is selected such as to avoid the transonic shock reflection back into the domain. Domain size was chosen as 75 times the diameter of the module for all simulated cases

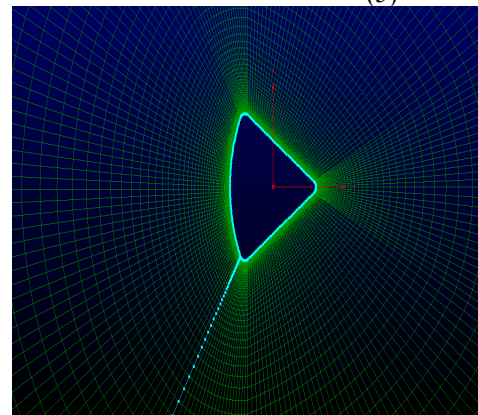


Figure 1. Zoomed cut plane view of the Grid over the re-entry module

Re-entry module was specified as a wall and the whole domain was specified as a Far field boundary condition. Dimensional details of the simulated model are given in Table 2.

Table 2: Dimension Details

BASE MODEL	R (SPHERICAL RADIUS)	θ (FLARE ANGLE)
D1	0.25 R	0.25 θ
D2	0.5 R	0.5 θ
D3	1.75 R	1.75 θ
D4	2 R	2 θ

where R represents the typical spherical radius and θ represents typical flare angle in a capsule.

Simulations were carried out for three different Mach numbers ranging from 1.2, 4, 6 for corresponding altitudes of 13, 25 and 28.7 km respectively and the corresponding ambient conditions were applied.

4. NUMERICAL SCHEME

CFD has been employed to analyze the flow over a re-entry module to obtain optimum design parameters such as nose radius and cone angle. Numerical simulations were carried out with a CFD code "SU2" with Navier-stokes k- ω SST turbulence model for various Mach numbers at an arbitrary altitude. For adding viscous effect Sutherland law was incorporated into the CFD solver. The results obtained from the numerical simulations were validated with analytical calculations.

5. RESULTS AND DISCUSSIONS

Numerical simulations have been carried out for different inlet Mach numbers to study the effects of design parameters on the flow characteristics. Fig.2 shows comparison of pressure behind the detached shock predicted using analytical and CFD methods.

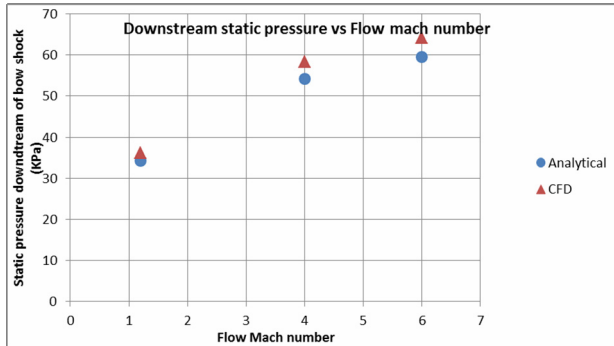


Figure 2. Comparison of static pressure downstream of the detached shock predicted using analytical and CFD methods

The results are validated with analytical calculation and also with the previous works published by Bruce Ralphin Rose et al [2]., which shows significant contributions for the validation of the current computational tool.

Initially the front spherical nose radius and flare cone angle were varied to study their effect over the entire module. At $M=1.2$, formation of vortices behind the capsule due to the wake flow field were observed and these vortices were found to diminish when the nose radius was lowered from D1 to D4 as shown in Fig-3.

The variation of C_p with the distance from the vehicle nose for various nose radii at $M = 1.2$ is highlighted in Fig 4. Initially the pressure was high due to stagnation and from C_p distribution it is clear that the increase in nose radius gradually decreased the pressure distribution at the nose cone and vice versa.

The flare angle also plays a major role in the downstream flow characteristics of a module. If the flare angle was increased, the length of the module decreased. As the flow turned around the shoulder of the re-entry module, it expanded rapidly and began to separate. Increase in flare angle increased the flow separation and the wake region formed downstream as shown in Figure 5.

At $M=4$, flow field around the forebody was dominated by a bow shock wave. Due to increase in nose radius the curvature of the bow shock increased and the pressure domination behind the bow shock decreased. Flow separation and formation of the vortices behind the capsule due to the wake flow field were less compared to the case with smaller nose radius as shown in Fig 6.

The variation of C_p with the distance from the vehicle nose for various nose radii at $M = 4$ are shown in Fig 7. Initially the pressure was high due to stagnation, but the initial pressure domination reduced when the nose cone radius was increased. And from C_p distribution it is clear that increase of nose radius gradually decreased the pressure distribution at the nose cone and decrease in nose radius suddenly decreased the pressure level at the end of a nose cone.

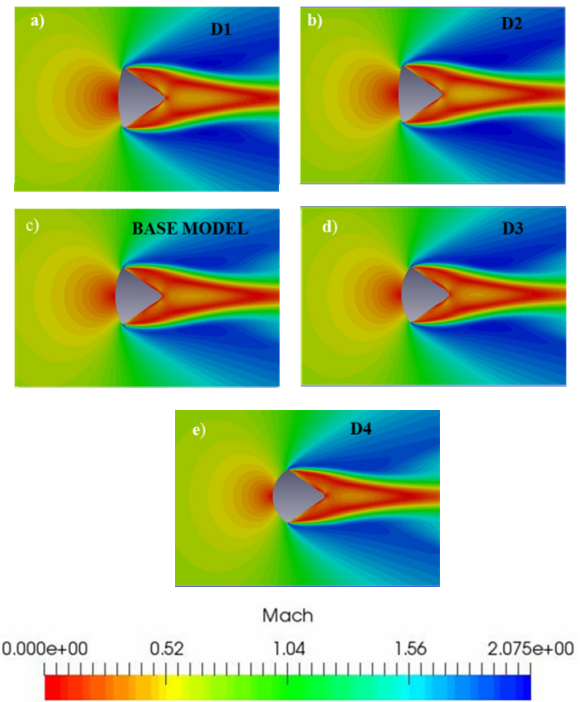


Figure 3. Mach distribution contour for different spherical nose radii at $M=1.2$

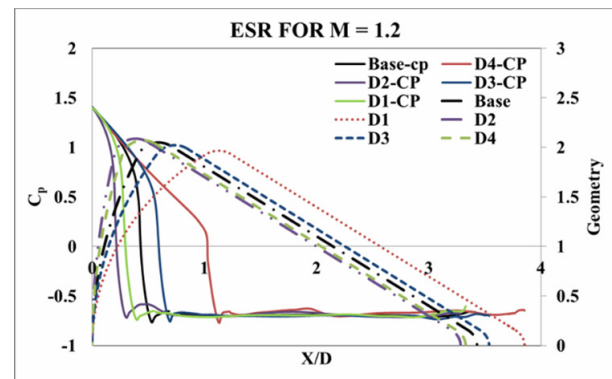


Figure 4. Plot showing the variation of C_p distribution with different spherical nose radii at $M=1.2$

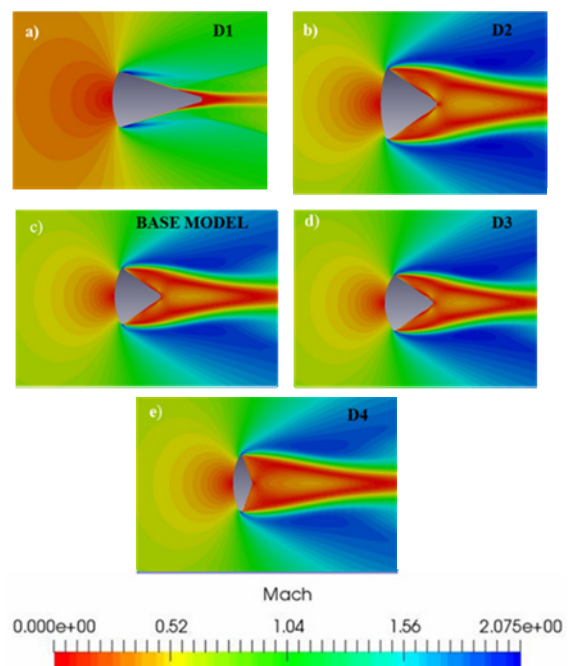


Figure 5. Mach contour for different flare angles at $M=1.2$

At $M=4$, flow field around the forebody was dominated by a bow shock wave. Due to increase in nose radius the curvature of the bow shock increased and the pressure domination behind the bow shock decreased. Flow separation and formation of the vortices behind the capsule due to the wake flow field were less compared to the case with smaller nose radius as shown in Fig 6.

The variation of C_p with the distance from the vehicle nose for various nose radii at $M = 4$ are shown in Fig 7. Initially the pressure was high due to stagnation, but the initial pressure domination reduced when the nose cone radius was increased. And from C_p distribution it is clear that increase of nose radius gradually decreased the pressure distribution at the nose cone and decrease in nose radius suddenly decreased the pressure level at the end of a nose cone.

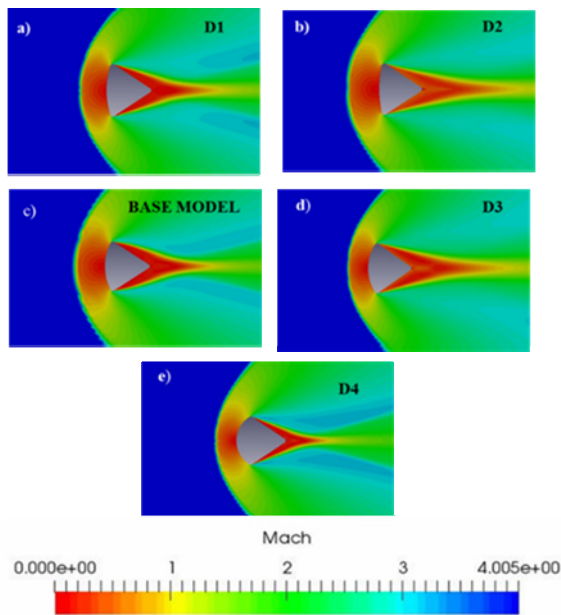


Figure 6. Mach distribution contours for different spherical nose radii at $M = 4$

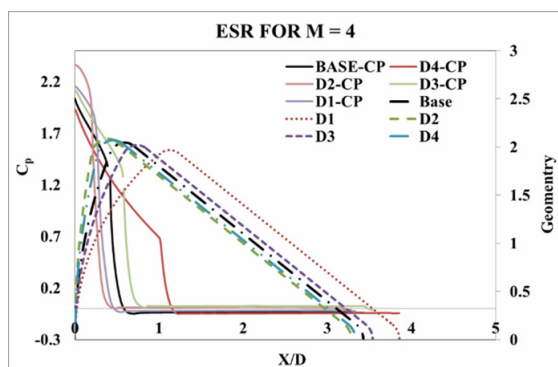


Figure 7. C_p distribution for different flare angles at $M=4$

The flare angle also plays a major role in the flow characteristics downstream of a module. If the flare angle was increased, at the fore body of a capsule the bow shock is formed and behind the bow shock the pressure domination will be higher for higher flare angle. When the flow turns around the shoulder of the capsule, it expands rapidly and began to separate. From C_p distribution it is clear that due to change of flare angle there is no significant change in pressure distribution over a re-entry module which can be seen in Fig 9.

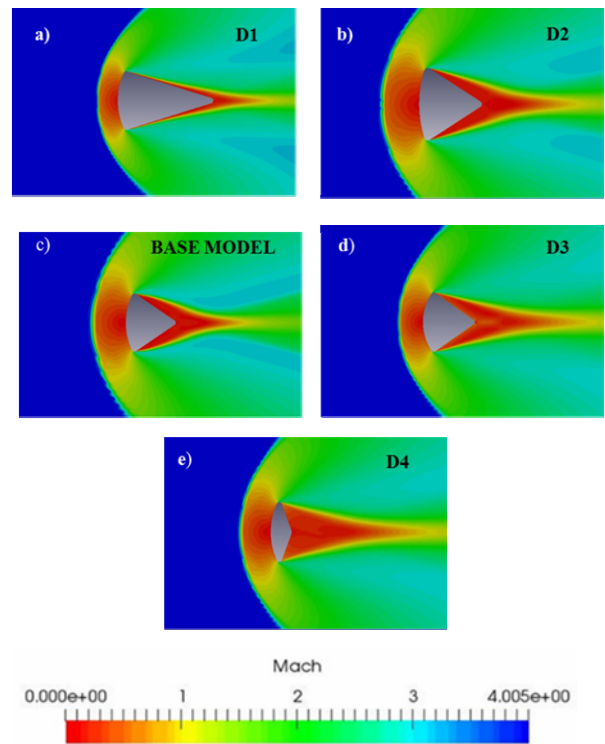


Figure 8. Mach contour for different flare angles at $M=4$

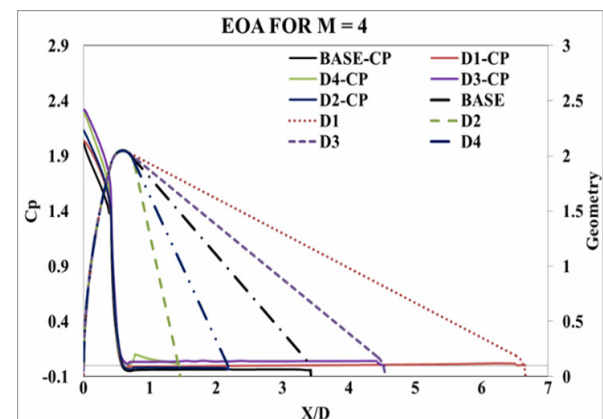


Figure 9. C_p distribution for different flare angles at $M=4$

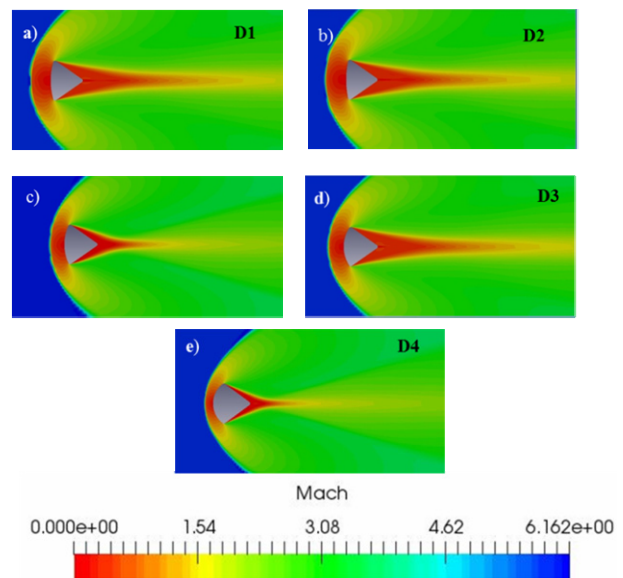


Figure 10. Mach distribution contour for different spherical nose radii at $M=6$

For hypersonic flow ($M=6$) the shock standoff distance was less compared to $M=4$. For $M=6$ the increase in spherical nose radius lowered flow separation and the wake region behind the capsule as shown in Fig 10.

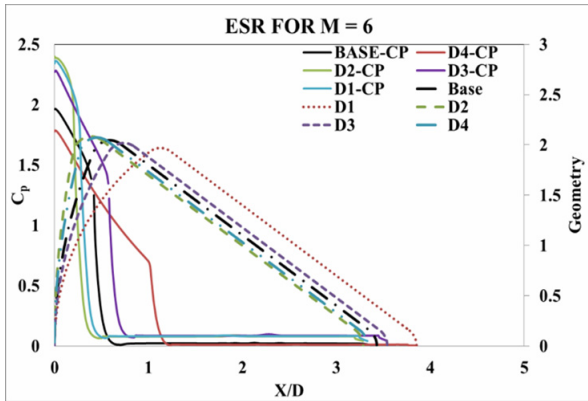


Figure 11. C_p distribution for different spherical nose radii at $M=6$

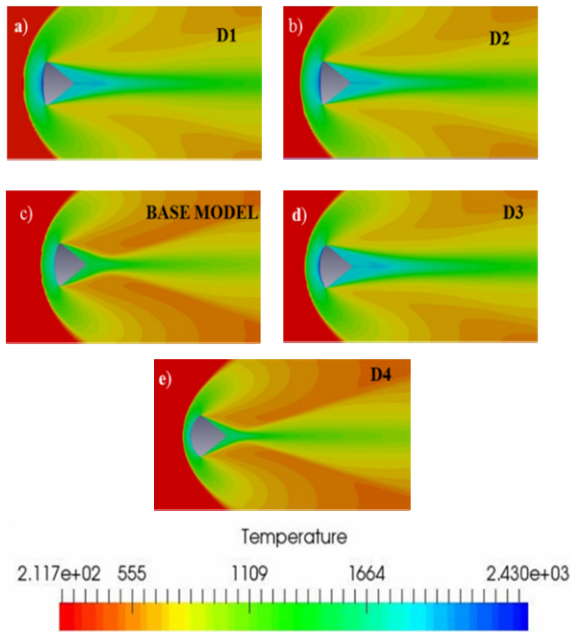


Figure 12. Temperature contour for different nose radii at $M=6$

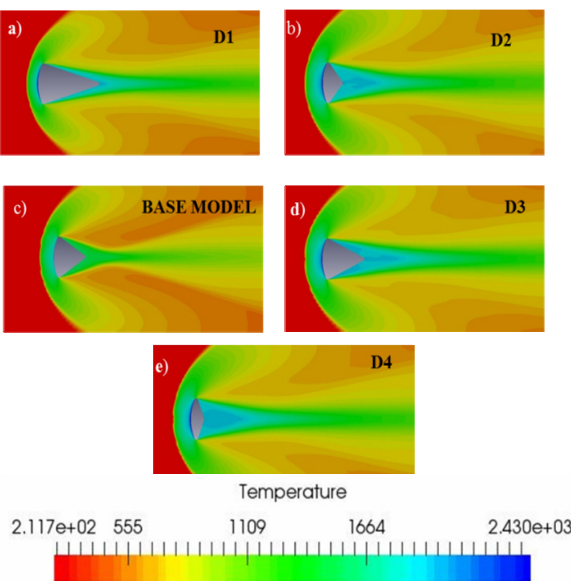


Figure 13. Temperature contours different flare angles at $M=6$

From the temperature contours it is evident that a change in flare angle, altered the temperature distribution by affecting the aerodynamic heating at Mach 6 as shown in Fig 13. The effect of the increase in flare angle also reduced flow separation behind the capsule as shown in Fig 14.

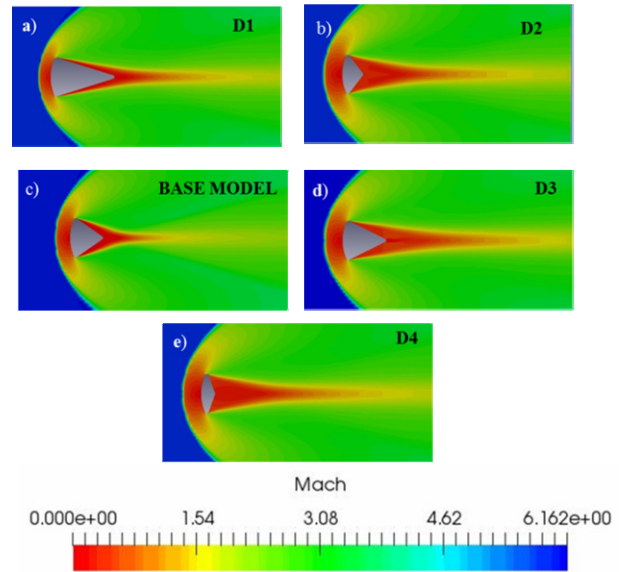


Fig 14: Mach contour for different flare angles at $M=6$

6. CONCLUSIONS

Numerical simulations were carried out for a re-entry vehicle in the supersonic and hypersonic flow regimes to compute the associated complex flow field, aerodynamic characteristics over the vehicle. Effects of the spherical nose radius and flare angle were captured using the open source code SU2. Significant observations were made in the course of the analysis to customize the flow properties around the vehicle. The analytical and CFD predictions of the pressure downstream of the bow shock were in good agreement. The variation in the flow field and pressure distribution over the module with the change in geometric parameters was observed. The high temperatures due to shock and viscous heating encountered in the re-entry regime were captured. From results it is clear that, due to the different spherical nose radii and flare angles there is a significant change in flow field both upstream and downstream to the vehicle. This poses a serious problem while designing the heat shield for the re-entry capsule. An overall picture of the influence of the capsule's geometry was explained.

REFERENCES

- [1] Mehta, R.C.: Computations of flow field over Apollo and OREX reentry modules at high speed, Indian Journal of Engineering & Materials Sciences, Vol 15, pp. 459-466, 2008.
- [2] Ralphin Rose, J. B., Saranya, P., Bibal Benifa, J. V.: Investigation of computational flow fields and aero acoustic characteristics over a re-entry command module, Journal of Aerospace Engineering, SAGE Publications, 2016.

- [3] Mathews, R.N., Shafeeque, A.P.: Hypersonic flow analysis on an atmospheric re-entry module, International Journal of Engineering Research and General Science, Volume 3, Issue 5, 2015.
- [4] Shiva Prasad, U., Srinivas, G.: Flow Simulation over Re-Entry Bodies at Supersonic & Hypersonic Speeds, International Journal of Engineering Research and Development, Volume 2, Issue 4, 2012.
- [5] Shafeeque A P.: CFD analysis on an atmospheric re-entry module, International Research Journal of Engineering and Technology, Volume: 04 Issue: 01, 2017.
- [6] Rathnavel, S., Dipankar Das, Bruce Ralphin Rose, J. , Haroon Rashid, K.: Numerical Simulation Over a Multi-body Launch Vehicle Module at various Transonic Mach numbers, FME Transactions, Vol 45 No 2 pp 9-15, 2017.
- [7] Premkumar, P. S., Senthilkumar, C., Elangovan, S., CharavarthyBaskar, S.: Optimization of Oil- Cooler Duct Position for a Pusher Type Turboprop, AIAA 2013-4331, 2013.
- [8] Premkumar, P.S., Ponnuchamy, O.: Computation of Aerodynamic Gust Response using the Open-Source SU2 Code, RAeS Applied Aerodynamics conference proceedings, ISBN Number 1-85768-371-4, 2016.
- [9] John Anderson: Fundamentals of Aerodynamics, McGraw-Hill Education; 6 edition, 2016.
- [10] Allen, J.S., Cheng, S.I.: Numerical Solutions of the Compressible Navier-Stokes Equations for Laminar Near Wake, Physics Fluids, Vol. 13, No 1, pp 37-52, 1970.

NOMENCLATURE

CFD	Computational Fluid Dynamics
EOA	Effect of flare angle
EOR	Effect of Spherical Nose Radius
CF	Convergence factor
C_p	Pressure coefficient
α	Angle of attack
M	Free Stream Mach Number
ρ	Density
u, v, w	Velocity components in x, y, z coordinates
\vec{v}	Velocity of the vector
\vec{n}	Unit normal vector
dS	Elemental surface area
Ω	Control volume
\vec{f}_e	Body force
τ	Viscous stress tensor

H	Total enthalpy
E	Total energy per unit mass
\dot{q}_h	Heat transfer per unit mass
U	Vector of conserved variables
Q_T	Heat flux
μ_i	Molecular viscosity
μ_t	Turbulent viscosity
n_x, n_y, n_z	Flux vector in x, y and z directions
μ	Viscosity coefficient
P	Pressure
e	Total internal energy
K	Thermal conductivity
T	Temperature
τ	Shear stress
γ	Ratio of specific heats
F	Flux vector

ИСТРАЖИВАЊЕ ИЗРАЧУНАВАЊА ПОЉА ВАЗДУШНЕ СТРУЈЕ НА ПОВРШИНИ КАПСУЛЕ ЗА ПОВРАТАК У ЗЕМЉИНУ АТМОСФЕРУ ПРИ ВЕЛИКОЈ БРЗИНИ

**С. Ратнавел, К. Балаји, П. Кумар П.С.,
Н. Сатеш Р., К.В. Санкаран**

Путовање у свемир са људском посадом је саставни део модерног света. Један од важних аспеката свемирских програма је безбедан повратак посаде на Земљу коришћењем капсуле за поновни улазак у атмосферу. Мисија поновног уласка у атмосферу је изузетно значајна јер се изводи брзином 30 пута већом од брзине звука и при високој температури која јонизује ваздух. Пројектовање капсуле мора да се врши изузетно пажљиво јер се ради о безбедности астронаута. Рад приказује симулације изведене на капсули за повратак у атмосферу у различитим условима слободног тока ваздушне струје: подзвучном, надзвучном и хиперсоничном режиму. Резултати су добијени помоћу Навије-Стоксових једначина за нестишљив флуид коришћењем к-омега модела турбуленције. Симулације су вршене при различитим улазним условима који одговарају висини на којој се налази капсула применом CFD кода SU2. Геометријски параметри капсуле: радијус сферног носа и угао конуса, су варирани, док су анализом обухваћени ефекти аеродинамичких појава: ударни талас, одвајање ваздушне струје и стварање турбулентног струјања на површини капсуле у правцу ваздушне струје. Приказани су резултати дистрибуције притиска, контуре Маховог броја и температура на површини капсуле.